Constraints on $f(R)$ and nDGP Modified Gravity Model Parameters with Cluster Abundances and Galaxy Clustering

Rayne Liu, Nicholas Battaglia, and Rachel Bean
Department of Astronomy, Cornell University, Ithaca, NY 14853, USA

Georgios Valogiannis
Department of Physics, Harvard University, Cambridge, MA 02138, USA

Mathew S. Madhavacheril
Perimeter Institute for Theoretical Physics, Waterloo, ON N2L 2Y5, Canada
(Dated: December 15, 2020)

We present the forecasted cosmological constraints from jointly combining data on galaxy cluster abundances from a future CMB-S4 experiment and galaxy clustering from a DESI-like experiment on two well-studied modified gravity models, the chameleon-screened $f(R)$ Hu-Sawicki model and the nDGP braneworld Vainshtein model.

A Fisher analysis is conducted using linear density perturbation information from σ_8 constraints derived from thermal Sunyaev-Zel'dovich (tSZ) selected galaxy clusters, as well as linear and mildly non-linear redshift-space 2-point galaxy correlation functions. We find that the cluster abundances drive the constraints on the nDGP model while $f(R)$ constraints are led by galaxy clustering. These two distinct tracers of the cosmological gravitational field are found to be complementary, and their combination significantly improves constraints on the $f(R)$ in particular in comparison to each individual tracer alone. For a fiducial model of $f(R)$ with $\log_{10} f_{R0} = -6$ and $n = 1$ we find combined constraints of $\sigma(\log_{10} f_{R0}) = 0.48$ and $\sigma(n) = 2.30$, while for the nDGP model with $n_{\rm nDGP} = 1$ we find $\sigma(n_{\rm nDGP}) = 0.087$. The results present the exciting potential to utilize upcoming galaxy and CMB survey data available in the near future to discern and/or constrain cosmic deviations from GR.

I. INTRODUCTION

The ΛCDM model accredits the acceleration of cosmic expansion to the negative pressure exerted by an unknown dark energy, with a canonical equation of state $w = -1$. However, more direct evidence for dark energy is still absent. The vacuum energy explanation proposed from the Standard Model in particle physics has suffered stark incompatibility with observations; the proceeding time-dependent dark energy field theories that attempt to resolve the discrepancy face fine-tuning problems.

Modified gravity (MG) theories attempt to avoid this extra energy component by explaining the accelerating universe with altering the law of gravity, namely Einstein's theory of General Relativity (GR) in large scales. Whilst GR has been more successfully tested with astrophysics in smaller scales such the solar system and strong-gravity regime, MG can potentially be applicable to larger cosmic scales with relatively weak gravitational fields. Nevertheless, such remarkable tests of GR in small scales have already imposed stringent constraints, leaving little free room for most MG models to develop. Two particularly well-studied MG models that survive are the Hu-Sawicki $f(R)$ model series [1], which feature a Chameleon mechanism, and the normal-branch Dvali-Gabadadze-Porrati braneworld model (nDGP) [2], which introduces a fifth dimensional force (Vainshtein mechanism). They successfully evade the above small-scale tests, while also reproducing an expansion history indistinguishable from ΛCDM. Hence, constraints via other independent observational quantities, especially the growth of the cosmic large-scale structure (LSS), are of crucial importance. Complementary to constraints via optical distance measurements on the expansion history, those features of growth are very sensitive to the cosmological models of interest.

Current and future cosmological surveys that observe the abundance of galaxy clusters, as well as the 3-dimensional positions and velocities of galaxy halos, can be a powerful probe of the LSS growth, and subsequently gravity and dark energy. In this work, we explore the constraining power of cluster abundances from tSZ observations by the Simons Observatory [3] and galaxy clustering from spectroscopic observations by the Dark Energy Spectroscopic Instrument (DESI) [4]. Galaxy clusters have long been regarded a promising set of observables to test modified gravity theories, and their abundances represented as number counts, as well as mass profiles, both serve as powerful tools. Measurements and selection of galaxy clusters have developed across multiple signal types including X-rays, the Sunyaev Zel'dovich (SZ) effect [5], and gravitational lensing. Some of the earlier works have already placed well-founded constraints on MG models such as $f(R)$ using data from the Planck satellite and the South Pole Telescope (SPT) [6].

In Section II we outline the theoretical and observational assumptions used in the analysis. We present the results of our analysis in Section III and finish with a discussion and implications for future work in Section IV.

II. FORMALISM

We describe the modified gravity models considered in the analysis in section II A. In section II B we discuss how the predictions for galaxy cluster abundances are used to estimate σ_8, while in II C we outline the method to predict redshift galaxy cluster correlations. The Fisher analysis approach is summarized in II D.

A. Modified Gravity Models

In this section we briefly introduce the MG models we examine and their effects on the growth of structure, which will motivate the constraint efforts. We focus our attention on two quintessential models in the literature of MG, the Hu-Sawicki $f(R)$ and the nDGP braneworld models, which respectively realize the Chameleon and Vainshtein classes of screening.

1. $f(R)$ Hu-Sawicki model

In the Hu-Sawicki $f(R)$ model, a nonlinear modification function, $f(R)$, of the Ricci scalar is added to the standard Einstein-Hilbert action:

$$S = \int d^4x\sqrt{-g}\left[\frac{R+f(R)}{16\pi G} + \mathcal{L}_m\right], \tag{1}$$

where G is the Newtonian gravitational constant, $\mathcal{L}_m$ the matter Lagrangian, and $f(R)$ induces the accelerating universe instead of a cosmological constant Λ. The growth equations are typically expressed in terms of the scalaron, $f_R \equiv \frac{df(R)}{dR}$, with a present day value

$$f_{R0} = -n\frac{c_1}{c_2^2}\left(\frac{\Omega_{m0}}{3(\Omega_{m0}+\Omega_{\Lambda 0})}\right)^{n+1}, \tag{2}$$

where Ω_{m0} and $\Omega_{\Lambda 0}$ are the normalized density parameters for nonrelativistic mass and dark energy today. These ΛCDM parameters appeared in the expression of the MG parameter as a result from imposing an expansion history identical to the ΛCDM scenario. It can be shown that through a conformal transformation, the Einstein frame expression (1) can be cast into the form of a scalar-tensor theory with the scalaron acting as the MG-induced degree of freedom [7]. In high curvature scales, i.e. $R \gg m^2$, the free parameters c_1, c_2 in (2) can be further constrained, effectively reducing the model parameters to the pair of f_{R0} (typically $|f_{R0}|$ in the literature, and for the rest of this paper we only consider cases where $f_{R0} > 0$) and n. We recover the ΛCDM (GR) model when $f_{R0} \to 0$, which is the case in regions of high Newtonian potential, where the chameleon field becomes very massive due to the effect of the screening mechanism [8, 9].

Extensive studies of the Hu-Sawicki model in the past decade have led to increasingly tighter constraints placed on the available parameter space of the model [10] [11], which however is still viable, and also happens to be devoid of any instabilities [12]. For all these reasons, it serves as the ideal test bed for us to explore constraints on MG with upcoming surveys of the LSS and CMB (as also considered by [13, 14]).

2. nDGP model

The Davli-Gabadadze-Porrati (DGP) model is a representative example of the Vainshtein screening mechanism [15, 16], and features a modification to gravity due to a large extra fifth dimension of spacetime. The modified Hilbert action is

$$S = \int d^4x\sqrt{-g}\left[\frac{R}{16\pi G} + \mathcal{L}_m\right] + \int d^5x\sqrt{-g_5}\frac{R_5}{16\pi G r_c}, \tag{3}$$

where R_5 and g_5 denote respectively the corresponding Ricci scalar and metric determinant of the fifth dimension, and r_c the cross-over distance, a characteristic scale below which GR model becomes four-dimensional. A more appealing self-accelerating DGP model branch (sDGP), which requires no dark energy, has been shown to suffer from undesirable instabilities [17], hence we study the "normal" branch (nDGP) coupled with a dark energy component to match the desired ΛCDM expansion history, which still remains interesting due to prior simulation investments. In this case, the only free parameter to constrain is $n = H_0 r_c$ (H_0 is the Hubble constant), of which the extensively studied values are 1 and 5. GR is recovered when $n \to \infty$, corresponding to the presence of large gradients of gravitational forces in Vainshtein screening.

B. Cluster Abundances and σ_8

The constraints by cluster abundances are modeled after results obtained in [3], in which a Fisher forecast based on galaxy clusters selected via the thermal SZ effect (tSZ) for a CMB Stage-4 experiment is extended to model-independent constraints on the time-evolution of $\sigma_8(z)$. σ_8 is the amplitude of matter energy density fluctuations smoothed out over a scale $R = 8Mpc/h$, and its evolution over redshift z is a promising probe of structure growth in the linear density perturbation regime.

To predict $\sigma_8(z)$ from MG models, we calculate σ_8 through the standard deviation of the probability density function of the matter density fluctuations, convoluted with a spherical top-hat window function $W(\mathbf{r}, R)$ with radius R:

$$W(\mathbf{r}, R) = \frac{1}{4\pi R^3/3} = \begin{cases} 1, & |\mathbf{r}| \le R, \\ 0, & |\mathbf{r}| > R. \end{cases} \tag{4}$$

Fourier transforming, Parseval's theorem gives

$$\sigma_R{}^2(z) = \int_0^\infty \frac{P(k,z)}{2\pi^2}\left[\frac{3j_1(kR)}{kR}\right]^2 k^2 dk, \qquad (5)$$

where $P(k,z)$ is the matter power spectrum at wavenumber k and redshift z, $j_1(kR)$ is the spherical Bessel function of the first kind, and $3j_1(kR)/(kR)$ is the Fourier transform of the window function.

In general, the power spectrum in MG can be obtained from the ΛCDM one by considering the modifications to the linear growth factor $D(k,z)$:

$$P_{\rm MG}(k,z) = P_{\Lambda\rm CDM}(k,z=0)\cdot\left(\frac{D_{\rm MG}(k,z)}{D_{\Lambda\rm CDM}(z=0)}\right)^2. \quad (6)$$

The growth factors, more commonly expressed as $D(k,a)$ ($a = 1/(1+z)$ is the scale factor), are obtained by solving the modified linear density evolution equations, extracted from the work of [18]:

$$\ddot{D} + 2H\dot{D} - 4\pi G\rho_m(1+g_{\rm eff})D = 0, \qquad (7)$$

where H is the Hubble parameter, ρ_m is the non-relativistic matter density, and dots are derivatives with respect to time t. The effective gravitational factor $g_{\rm eff}$ is, for $f(R)$ and nDGP respectively,

$$g_{\rm eff} = \frac{k^2}{3(k^2 + a^2 m(a))^2} \qquad (8)$$

with the associated mass term

$$m(a) = \frac{1}{c}\sqrt{\frac{[\Omega_{m,0} + 4(1-\Omega_{m,0})]^{-(n+1)}}{(n+1)|f_{R0}|}} \times \sqrt{\left[\frac{\Omega_{m,0}}{a^3} + 4(1-\Omega_{m,0})\right]^{n+2}}, \qquad (9)$$

and

$$g_{\rm eff} = \frac{1}{3\beta(a)} \qquad (10)$$

where

$$\beta(a) = 1 + 2Hr_c\left(1 + \frac{\dot{H}}{3H^2}\right) = 1 + 2\frac{H}{H_0}n\left(1 + \frac{\dot{H}}{3H^2}\right). \qquad (11)$$

Comparing (8) and (9) to (10) and (11), we can see the linear growth factor D depends on both k and a in $f(R)$, and is scale independent in nDGP. Hence, σ_8 acts as a convenient tool for intuitively comparing models with different scale dependence, since the scales are marginalized over in the calculation of σ_8. For more direct comparison with the standard ΛCDM model, we evaluate $\sigma_{8(\rm MG)}/\sigma_{8(\Lambda\rm CDM)}$ as predicted by the above equations. We obtain the ΛCDM linear matter power spectrum at redshift zero, $P_{\Lambda\rm CDM}(k, z = 0)$, from the Boltzmann code CAMB [19–21] as a starting point, and then utilize (5) and (6) to determine $\sigma_{8(\rm MG)}/\sigma_{8(\Lambda\rm CDM)}$. Based on the assumptions in MG, the structure growth at early times should be indistinguishable from that in ΛCDM, hence we normalize the ratio to 1 at redshift $z = 10$, high enough to set the initial conditions of structure growth. We also note a slight discrepancy on the growth factors between the GR limit solution of (7) and the ΛCDM prediction from CAMB, which are far below the statistical uncertainities to affect the results of the Fisher analysis, and are corrected by normalization using the former.

Our solution of $D(k,a)$ for the $f(R)$ model is checked against the work of [22] in which the code for linear perturbation in MG is slightly modified for our purpose. Our solutions of $D(a)$, for both the ΛCDM and the nDGP models, are checked against the empirical fitting function proposed by [23]:

$$g(a) \equiv D(a)/a = \exp\left[\int_0^a \frac{da'}{a'}\left[\Omega_m(a')^\gamma - 1\right]\right], \quad (12)$$

where $\Omega_m(a) = \Omega_{m0}a^{-3}/(H/H_0)^2$, $\gamma = 0.55$ for ΛCDM and 0.68 for DGP with a modified expansion history [23]. This agreement remains stable when Ω_{m0} is varied in a small range around our fiducial value $\Omega_{m0} \sim 0.315$. In our work after the check, the ΛCDM expansion history (Hubble parameter) is imposed on the nDGP model.

We briefly note on the advantages of using σ_8 to represent constraints from cluster abundances. Although the constraints are compressed into a root-mean-squared quantity as σ_8, not much information is lost since we are examining the linear regime. On the other hand, to implement a full analysis with the galaxy clusters mass function, further numerical simulation is required. In comparison, performing a Fisher analysis using σ_8 based on [3] is not only faster, but also more conservative in the sense that it does not introduce extra degeneracy breaking as is the case for a detailed numerical simulation.

C. Galaxy Clustering Correlations

The LSS of the universe, as traced by the observed inhomogeneous clustering pattern of galaxies, has been formed by the nonlinear gravitational collapse of the primordial density distribution. We can model the observed clustering statistics of galaxies in MG, by taking into account the crucial effects of non-linear clustering, large-scale galaxy bias and redshift space distortions (RSD). Our modeling procedure, which is tailored to DESI observations, is summarized below, and is heavily based upon the previous works of [24, 25].

In the intermediate, quasi-linear scales higher order perturbation theory can substantially improve upon the accuracy of the simple linear treatment, allowing for a robust modeling of the clustering statistics, without the need to resort to computationally expensive N-body simulations. In this work we will focus on Lagrangian perturbation theory, in which the expansion parameter is a vector field, $\mathbf{\Psi}$, which displaces each fluid particle from its initial position, $\mathbf{q}$, to its final, Eulerian one, $\mathbf{x}(\mathbf{q},t)$, through the mapping:

$$\mathbf{x}(\mathbf{q},t) = \mathbf{q} + \mathbf{\Psi}(\mathbf{q},t). \tag{13}$$

The first order LPT solution is the famous Zel'dovich approximation [26]. In MG theories, an additional degree of freedom is present, altering the perturbed Einstein equations and the nonlinear gravitational evolution of dark matter overdensities, and subsequently the framework of LPT, as detailed in [24, 27–29].

The galaxies observed by surveys of the LSS do not perfectly trace the underlying dark matter density distribution, but rather are biased tracers of it [30]. In the simpler picture of linear perturbation theory, the large-scale overdensity of biased tracers (i.e. galaxies) is proportional to the underlying dark matter overdensity [31], while a wide range of more sophisticated treatments have been developed in the literature [32]. When working in Lagrangian space, in particular, as we do in this work, biased tracers are identified as regions of the primordial density field that are pre-selected by a biasing function, F, that depends on the local matter density [33, 34]. Given the statistical nature of cosmic density fields, the simplest meaningful observable statistic (in the configuration space) is the two-point correlation function, $\xi_X(r)$, of tracers correlated over a distance r:

$$\xi_X(r) := \langle \delta_X(\mathbf{x})\delta_X(\mathbf{x}+\mathbf{r})\rangle, \tag{14}$$

where the angle brackets denote an ensemble average. Working in Lagrangian space, "Convolution Lagrangian Perturbation Theory" (CLPT) [34–36] was shown to work particularly well at recovering the correlation function of halos from N-body simulations, in ΛCDM cosmologies. Building upon these works, [24, 28] then expanded CLPT in the case of MG theories and successfully recovered the real-space two-point correlation function of dark matter haloes across the parameter space of the $f(R)$ and nDGP MG scenarios.

In addition to imperfectly tracing the dark matter distribution of the cosmic web, galaxies identified through spectroscopic means are observed in redshift space, rather than in the real space, which further distorts the observed clustering pattern; the Redshift Space Distortions (RSD) [37–39]: due to its peculiar velocity about the Hubble flow, $\mathbf{v}(\mathbf{x})$, a galaxy with real space position $\mathbf{x}$ will be instead observed at a redshift space position:

$$\mathbf{s} = \mathbf{x} + \frac{\hat{z}\cdot\mathbf{v}(\mathbf{x})}{aH(a)}\hat{z}, \tag{15}$$

with $H(a)$ the Hubble factor at a given scale-factor a. As a consequence, the redshift-space 2-point correlation function for biased tracers

$$\xi^s_X(\mathbf{r}) = \langle \delta_X(\mathbf{s})\delta_X(\mathbf{s}+\mathbf{r})\rangle, \tag{16}$$

becomes directionally dependent, unlike the real-space expression (14). In large linear scales, coherent infall leads to the "Kaiser boost", an enhancement on the amplitude of the two-point correlation function, whereas in the non-linear scales, the random velocities within virialized structures lead to the "Fingers-Of-God" (FOG) suppression effect.

The Gaussian Streaming Model (GSM) [40–42] has been shown to be very successful at modeling the anisotropic RSD correlation function of halos, through a convolution of the halo real space correlation function with the probability velocity distribution of tracers, that is approximated as a Gaussian [43]. In particular, given the real-space mean pairwise velocity along the pair separation vector of a pair of tracers, $v_{12}(r)$, as well as its pairwise velocity dispersion, $\sigma^2_{12}(r)$, then the GSM gives the follow expression for the anisotropic RSD correlation function:

$$1 + \xi^s_X(s_\perp, s_\parallel) = \int_{-\infty}^{\infty} \frac{dy}{\sqrt{2\pi\sigma^2_{12}(\mathbf{r})}}[1 + \xi^r_X(r)] \times \exp\left[-\frac{\left(s_\parallel - y - \mu v_{12}(r)\right)^2}{2\sigma^2_{12}(\mathbf{r})}\right], \tag{17}$$

where $s_\perp, s_\parallel$ are the perpendicular and parallel to the line-of-sight components of the redshift-space separation s, with $s = \sqrt{s^2_\perp + s^2_\parallel}$, $r = \sqrt{s^2_\perp + y^2}$ and $\mu = \hat{r}\cdot\hat{z} = \frac{y}{r}$. Using CLPT to model the 3 ingredients that enter the prescription (17), $\xi^r_X(r), v_{12}(r), \sigma^2_{12}(\mathbf{r})$, and based on the MG implementations of [24, 28], [44] was able to successfully model the simulated RSD correlation function of haloes in the $f(R)$ and nDGP gravity scenarios up to 1-loop order in PT. We note that, for the purposes of this work, we only use the 1^{st} order LPT solution (Zel'dovich approximation [26]) to evaluate the GSM ingredients, mainly because our model for the evaluation of the clustering covariance matrix does not incorporate non-Gaussian corrections, as we explain in the Appendix A.

Our final aim for this section is to model the observed RSD two-point correlation function of galaxies in MG (and ΛCDM) for a survey such as DESI, using the CLPT & GSM framework laid out in this section. Before we are able to reach this goal, however, we point out that the elements entering the final GSM expression (17) also depend, in addition to the known LPT growth factors and the linear power spectrum, on the Lagrangian bias parameters up to second order (for an 1-loop prediction), b^L_1 and b^L_2, that we also need to account for. In our DESI-type investigation, and as we will explain in greater detail in the following section, we will consider constraints from two types of objects, the Luminous Red Galaxies (LRGs) and the Emission Line Galaxies (ELGs), following [45]. For these two types of objects, the linear Eulerian galaxy bias can be modeled as [45, 46]:

$$b^E_1(z)D(z) = \begin{cases} 1.7, & LRG, \\ 0.84, & ELG, \end{cases} \tag{18}$$

where $D(z)$ is the ΛCDM linear growth factor, normalized to be unity at $z = 0$. The 2^{nd} order bias parameter is not treated as an independent parameter, but is rather determined in terms of the b_1^E prediction from eq. (18), through the fitting formula

$$b_2^E = 0.412 - 2.143 b_1^E + 0.929 (b_1^E)^2 + 0.008 (b_1^E)^3, \quad (19)$$

that has been calibrated from N-body simulations [47]. Finally, the Eulerian bias values b_1^E and b_2^E can be converted to the corresponding ones in the Lagrangian space, through the following known conversion relationships [48, 49]:

$$\begin{aligned} b_1^L &= = b_1^E - 1, \\ b_2^L &= = b_2^E - \frac{8}{21} b_1^L. \end{aligned} \quad (20)$$

Combining eqs. (18-20), we can finally determine the necessary bias parameters for a given galaxy sample and redshift z in terms of the linear bias, that we treat as a nuissance parameter, that we marginalize over, as we explain in the next section.

The second nuisance parameter we include is a constant offset, α_σ, that needs to be added to the modeled galaxy pairwise velocity dispersion,

$$\sigma_{12}^2 \to \sigma_{12}^2 + \alpha_\sigma, \quad (21)$$

such that the latter matches the observed prediction from simulations (or observations) at the large scale limit, as we found in [44]. This correction aims to capture unknown small-scale nonlinear effects and is essentially the equivalent of the 'Fingers-of-God' free parameter, σ_{FoG}^2, that is commonly employed in the simple phenomenological dispersion models [50, 51].

Finally, all of the above ingredients are combined to produce a prediction, by means of eq. (17), for the MG RSD galaxy correlation function for the ELG and the LRG DESI galaxy samples at a given redshift z. As commonly performed in the literature, we further decompose the correlation function through a multipole expansion in a basis of Legendre polynomials, $L_l(\mu_s)$:

$$\xi(s, \mu_s) = \sum_l \xi_l(s) L_l(\mu_s), \quad (22)$$

where the multiples of order l will be given by

$$\xi_l(s) = \frac{2l+1}{2} \int_{-1}^{1} d\mu_s \xi(s, \mu_s) L_l(\mu_s), \quad (23)$$

with $\mu_s = \hat{z} \cdot \hat{s} = s_\parallel / s$. We restrict our analysis on values $l = \{0, 2, 4\}$, which correspond to the monopole, the quadrupole and the hexadecapole, respectively (first 3 non-vanishing multipoles).

D. Fisher Analysis

In this section we proceed to obtain cross-correlated Fisher constraints on the parameters of the two MG models using tracers of the LSS, e.g. cluster abundances in the linear regime and nonlinear galaxy clustering.

	Parameter	Fiducial Value(s)
ΛCDM	$\Omega_c h^2$	0.1194
	$\Omega_b h^2$	0.022
	H_0	67.0
	$10^9 A_s$	2.2
	n_s	0.96
$f(R)$	f_{R0}	$10^{-5}, 10^{-6}, 0$
	n	1
nDGP	n_{DGP}	$1, 5$
Nuisance parameters	$b_1(z)$	Eq. (18)
	α_σ	0.5

TABLE I. The fiducial cosmological parameters for the background cosmology considered in the analysis and the baseline $f(R)$ and nDGP modified gravity scenarios. We add that the nuisance parameters refer only to the galaxy clustering evaluation.

Our adopted fiducial background cosmology and modified gravity parameters are shown in Table I, following [3]. We consider three different $f(R)$ scenarios with $f_{R0} = 10^{-5}$ (referred to as "F5"), 10^{-6} ("F6") and 0 (referred to as "near GR"). In the near-GR case, the parameter n becomes ill-defined at f_{R0}, so we consider its value as fixed at $n = 1$ and do not include it as a Fisher parameter. Furthermore, we consider two nDGP scenarios for $n = \{1, 5\}$, that we refer to as N1 and N1, respectively.

We utilize the Fisher formalism [52, 53] , assuming a Gaussian likelihood distribution:

$$F_{ij} = \sum_{\alpha\beta} \frac{\partial f_\alpha}{\partial p_i} Cov^{-1}[f_\alpha, f_\beta] \frac{\partial f_\beta}{\partial p_j}, \quad (24)$$

where f_α are the observables in bins labeled by α; Cov is the observable covariance matrix and p_i and p_j are a pair of the model parameters being constrained.

Constraints by cluster abundances, as discussed in II B, are represented by $\sigma_8(z)$. In particular, the observables f_α are the set of $\{\sigma_{8(\mathrm{MG})}(z)/\sigma_{8(\Lambda\mathrm{CDM})}(z)\}$ across 30 redshift bins within $z = 0.05 \sim 2.95$, which are predicted by the MG models. The error covariance matrix $Cov^{-1}[f_\alpha, f_\beta]$ on $\sigma_8/\sigma_{8(\Lambda\mathrm{CDM})}$, obtained in [3]

For the galaxy clustering the observables are the galaxy correlation function multipoles, $f_\alpha = \{\xi_0(s), \xi_2(s), \xi_4(s)\}$, considered over 35 spatial separation bins equally (logarithmically) spaced in the range $25 < s < 600$ Mpc/h. The cosmological parameters, p_i, are those given in Table I, while the covariance matrix for the monopole, quadrupole and hexadecapole moments is described in the Appendix A. Our evaluation assumes a DESI-like survey with LRG and ELG galaxy samples in the redshift range $0.15 < z < 1.85$, using 18 linearly spaced z bins, as outlined in [45]. Our choices for the galaxy number density, survey volume and linear bias as a function of redshift are informed by the above referenced work (in particular Table V in that paper). The partial derivatives of the multipoles are evaluated with a 2-point central differences scheme, with the derivative step-sizes with respect to the background ΛCDM parameters and linear bias provided by [3]. With regards to the MG gravity parameters, the derivative steps for the $\{f_{R0}, n\}$ pair in the F5 and F5 cases are $\{2 \times 10^{-6}, 0.4\}$ and $\{3 \times 10^{-7}, 0.4\}$, respectively, with the corresponding values for n in the N1 and N1 models being 0.15 and 0.5. In the near-GR case with $f_{R0} \to 0$, however, we cannot use central differences around the fiducial anymore, given the restriction $f_{R0} > 0$. In that case we employ a 3-point forward differences scheme instead, with a forward step of 10^{-8} in f_{R0} (while keeping n fixed). The step-size when differentiating with respect to the nuisance parameter α_σ is 1.5, informed by the detailed study performed in [44]. We have carefully checked and confirmed that all of the choices above provide numerical stability in the derivatives.

III. RESULTS

Having laid out the details of our Fisher forecasting setup in the previous section, we now proceed to present the predicted constraints on the cosmological parameters of Table I.

Starting with the galaxy clustering case of the ELG and LRG galaxy samples, in Figures 1 and 2 we consider the sensitivity of the cosmological constraints for the F5 and F6 cosmologies, respectively. In Figure 1, in particular, we present 2-dimensional constraints from each parameter pair in the Fisher analysis, as obtained by the first 3 non-vanishing multipoles of the redshift-space correlation function of the two galaxy samples, both when considered separately and also combined. In addition to the constraints on the standard ΛCDM parameters, which are in line with previous works in the literature (e.g. [45]), the complementarity of the LRG and the ELG-derived contributions allows us to tightly constrain the pair of the MG parameters $\{f_{R0}, n\}$, that are the focus of this analysis. As a result of this complementarity, the combined constraints from the two samples on the MG parameters are much tighter than the individual ones. The fact that using the ELGs produces tighter constraints in all parameter planes is totally expected, given that this sample has a larger number density and redshift range, compared to the LRG counterpart (see Table V of [45]).

Furthermore, as can be seen in Fig. 1, and as we further quantify in Table II, the forecasted constraints on the MG parameter f_{R0} are at least an order of magnitude tighter, relatively, compared to parameter n. This finding is attributed to the fact that the 2-point function is more sensitive to variations of f_{R0} than of n, in particular for the range of scales we consider in this work, as was found by the sensitivity analysis of [14]. Due to this fact, most previous works in the literature (e.g. [22, 54]) have commonly worked with a fixed value of $n = 1$, and only considered constraints to f_{R0}. Thanks to our flexible analytical model for the anisotropic correlation function in any scalar-tensor theory, in this work we produce constraints on the full parameter space of the f(R) Hu-Sawicki model, for the first time in the literature.

Last but not least, in Figure 1 we demonstrate how the choice of the minimum scale impacts the constraints we obtain, finding that a more conservative value of $r_{min} = 44Mpc/h$ dilutes the constraining power overall. This is once again expected, given that predicted deviations in the Hu-Sawicki model become progressively more pronounced, the smaller the scales we consider. As a result, focusing our analysis on larger scales restricts our ability to probe MG signals, resulting in looser constraints on the corresponding MG parameters. In Fig. 2 we repeat the same analysis as in Fig. 1, but for the smaller deviation F5 scenario, finding qualitatively similar results as in the F5 case. The only notable difference is that the predicted constraints to the two MG parameters are relatively looser, compared to the previous case, as is also shown in Table II. In a similar manner as above, this trend is consistent, when we consider that the predicted deviations, and as a result the overall constraining power in the correlation function, are smaller in the F6 scenario.

In Figure 3 we present the galaxy clustering constraints for the "near GR" scenario of $f_{R0} = 0$, finding overall a similar behavior as in the previous cases above. The main difference here lies in the fact that derivatives w.r.t. to the MG parameter n are ill-defined, as explained in Section II D, allowing us to only constrain deviations away from $f_{R0} = 0$. Nevertheless, the default assumption is commonly that of a ΛCDM fiducial cosmology, making this scenario a more realistic one in the context of upcoming surveys of the LSS and CMB. As shown in Fig. 3 and also Table II, combining the contributions from the ELG and the LRG samples will allow us to tightly constrain deviations away from GR, demonstrating the promise spectroscopic observations by DESI. Our constraints are of the same order as the ones presented in [54], that performed Markov Chain Monte Carlo analysis. We finally present the corresponding one-dimensional Gaussian constraint on f_{R0} in Figure 7, for the sake of completeness.

In addition, we note that we performed the same analysis, as the one above, for the second MG scenario under consideration, the nDGP model. For the sake of brevity, however, we will only present the final combined constraints and omit showing the full corner plots in this case. Having said that, we add that our findings are broadly very similar with the $f(R)$ scenario, that we discussed in detail above.

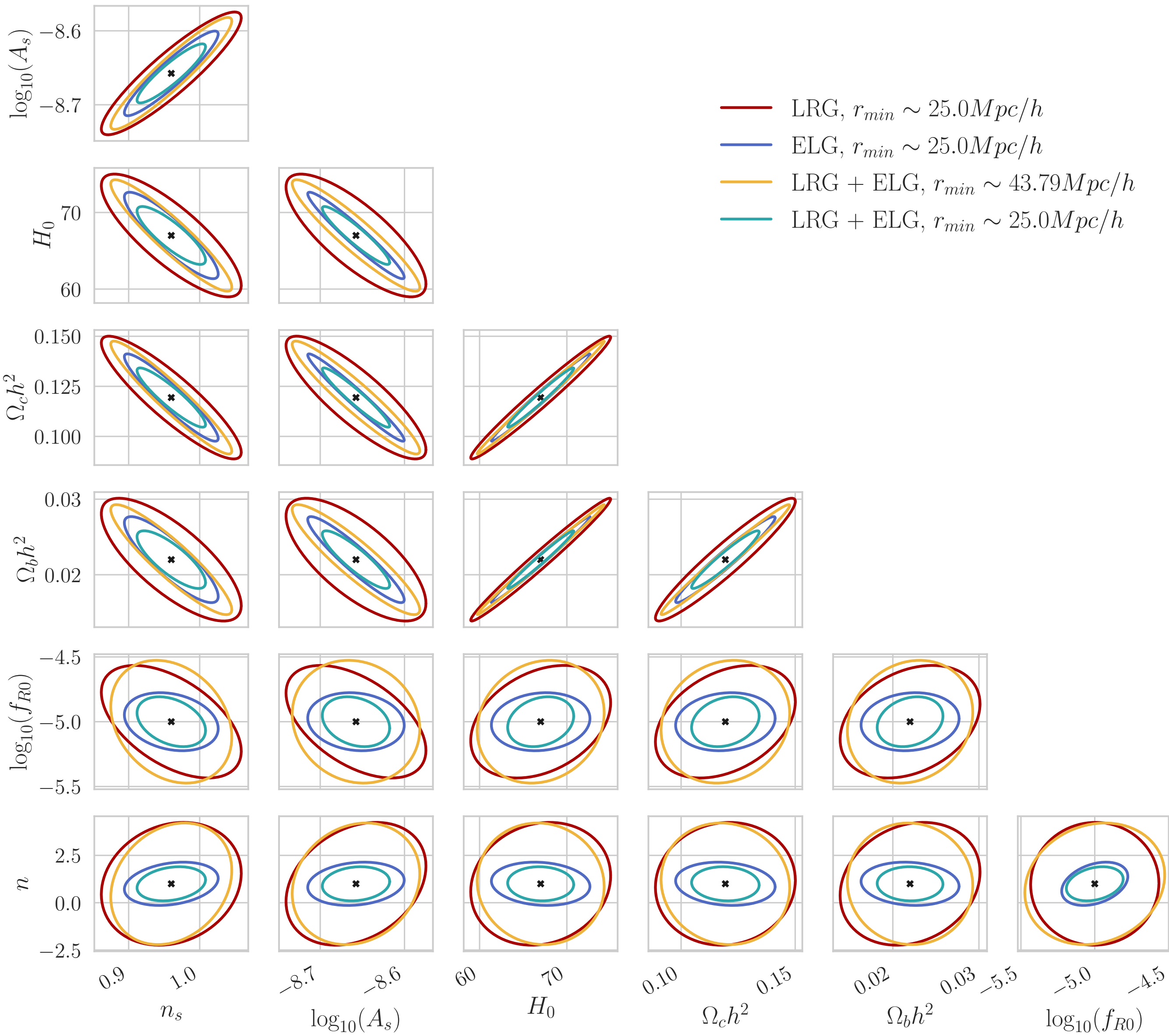

FIG. 1. Constraints on the parameters in the F5 case (fiducial values $f_{R0} = 10^{-5}, n = 1$). Note in this case we also included the results where $r_{min} \sim 43.79Mpc/h$, to demonstrate how such a choice gives a significantly looser constraint, as compared to the commonly chosen $r_{min} \sim 25.0Mpc/h$, which is the smallest scale-cut that can be realistically probed with surveys.

Moving on to discuss the constraints from cluster abundances, we first present in Figure 4 an overview comparison of the evolution of $\sigma_{8(\mathrm{MG})}/\sigma_{8(\Lambda\mathrm{CDM})}$ over the 30 redshift bins from $z = 0.05$ up to $z = 2.95$ predicted by the MG models vs. the forecasted errors from [3]. The plotted ratios are all normalized at $z = 10$, varying $\{f_{R0}, n\}$ for $f(R)$ and n for nDGP, respectively. The $\sigma_{8(\Lambda\mathrm{CDM})}$ is normalized to be that calculated from (7). The ratios are plotted together with the forecasted errors on $\sigma_{8(\mathrm{MG})}/\sigma_{8(\Lambda\mathrm{CDM})}$ via the cluster abundance error estimation for future CMB S-4 experiments obtained in [3]. This overview allows us to shed light on the sensitivity of σ_8 with respect to the corresponding parameters of the two MG models we consider. For both MG models, the constraining power mainly lies at lower redshifts of $z < 2$, where the deviation of the MG-predicted σ_8 is the highest, and the forecasted errors by cluster abundances are the tightest. Furthermore, by comparing the signal to errors for the $f(R)$ case in sub-figures (a) and (b), we anticipate that the σ_8 data will be far more sensitive to variations in f_{R0} than in n, as we also found to be the case with galaxy clustering. Based on sub-figure (c), lastly, σ_8 is also anticipated to give comparably tight constraints on the parameter n_{DGP} of the nDGP model.

We then examine the constraints provided by the Fisher analysis, both from the cluster abundances in and

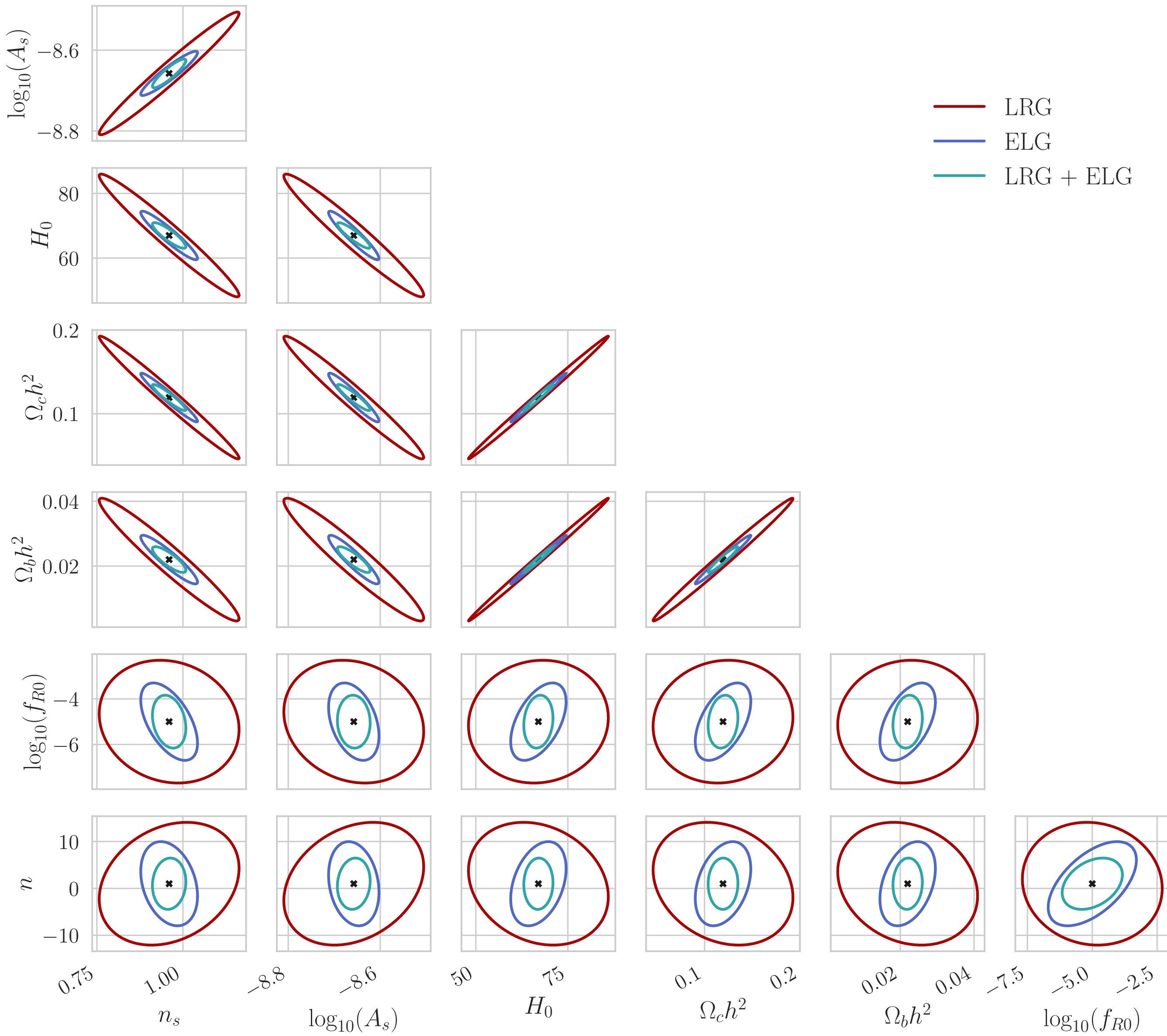

FIG. 2. Galaxy clustering constraints on the parameters in the F6 case (fiducial values $f_{R0} = 10^{-6}, n = 1$).

of themselves but also combined with the galaxy clustering results that we previously described. Since the ΛCDM parameter errors have already been marginalized over in the σ_8 case, we only present covariance ellipses on the key parameter plane of the pair $\{f_{R0}, n\}$ in the $f(R)$ scenario, which are shown in Fig. 5. We additionally present the profiles for the $1-\sigma$ confidence level plots for the MG parameters in the same figure, while the values of the marginalized errors are reported in Table II. We find that cluster abundances give very degenerate constraints on the $f(R)$ parameters as shown in the covariance ellipses, and this phenomenon has been tested to be relatively stable across all redshift ranges. The size of the covariance ellipses in respective redshift ranges in our test also confirms that the constraining power of cluster abundances mainly lies in the low redshift range. The results are on a similar order of magnitude with the galaxy clustering information presented previously, and when they are combined, we can further tighten the constraints in all cases considered, and for all the corresponding MG parameters. This demonstrates the great complementarity between these two distinct probes of the LSS.

The same conclusions can be drawn in the nDGP case, the 1-d constraints on which are presented in Fig. 6 and Table II, with the combined constraining power of the two probes being able to significantly narrow down the available parameter space of this model, for both fiducial cases of $n = 1$ and $n = 5$ that we consider. It is worth emphasizing, at this point, that, as we have already pointed

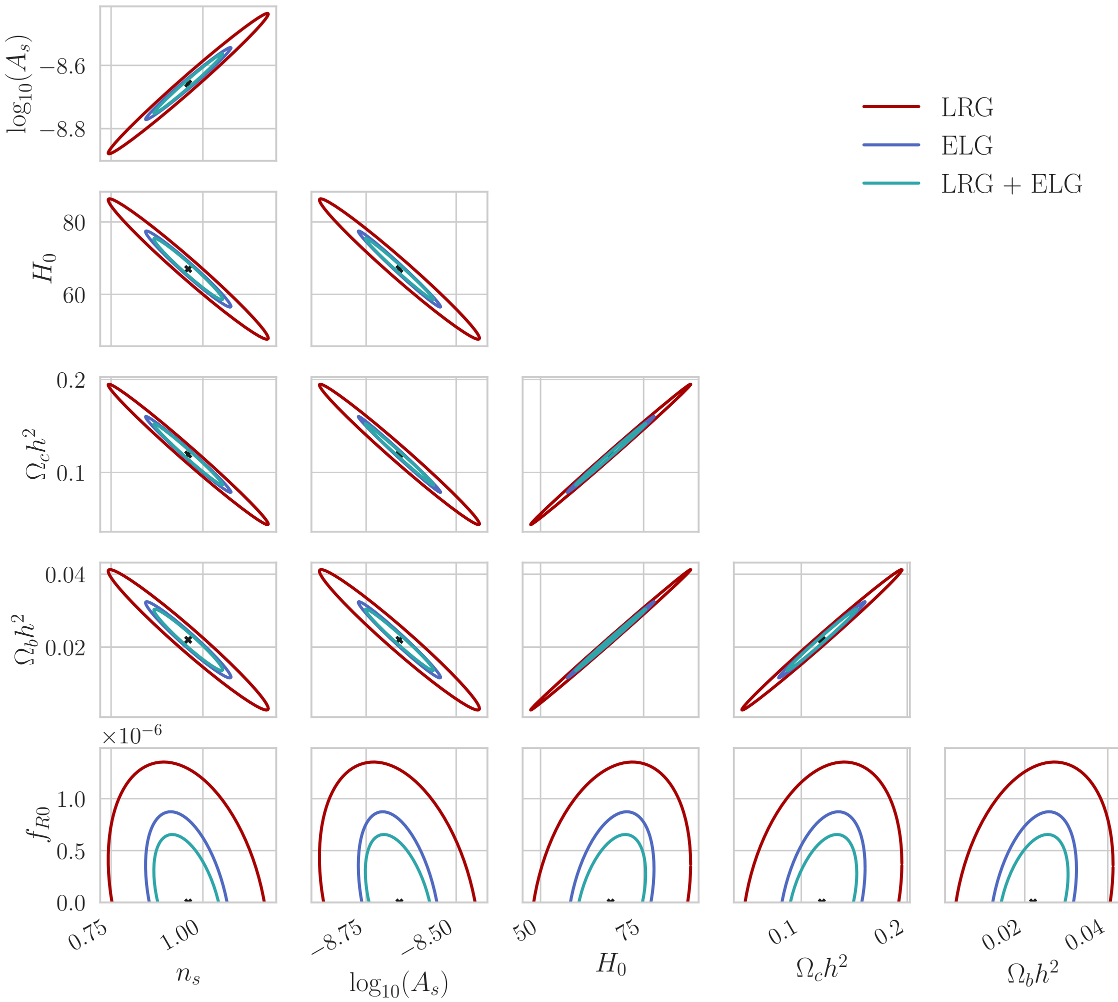

FIG. 3. Constraints on the parameters in the near-GR limit (fiducial values $f_{R0} = 0, n = 1$. The covariance ellipses regarding the constraints on f_{R0} show only the positive side.

out, the nDGP model realizes the Vainshtein screening mechanism, which is harder to constrain using other astrophysical probes, as opposed to the chameleon screening of the f(R) scenario; a fact that further highlights the importance of our findings.

Spanning the two most popular classes of screening in the literature, through the representative f(R) and nDGP MG models, our detailed analysis overall serves to highlight the ways in which the upcoming precise observations of redshift-space galaxy clustering and cluster abundances will enable us to probe the landscape of dark energy and modified gravity parametrizations in the next 10 years.

IV. DISCUSSION

In this work we performed a detailed study of our ability to constrain the large-scale properties of gravity with a combination of two promising probes of the LSS: galaxy clustering from spectroscopic observations by DESI, as well as cluster abundances from tSZ observations by the Simons Observatory.

On the galaxy clustering front, we employ the Gaussian Streaming Model with Lagrangian PT to predict the anisotropic redshift-space 2-point correlation function of biased tracers, that was recently generalized to support predictions for modified gravity parametrizations. We apply the model to predict the multipoles of the RSD correlation function for the ELG and the LRG DESI spectroscopic galaxy samples, as well as their corresponding covariance matrices. With regards to the cluster abundances, we use the amplitude of density fluctuations, σ_8, obtained by tSZ-selected galaxy clusters, as a window into the nature of the underlying gravity model, expanding upon recent detailed studies in the context of standard cosmologies.

We then employ the Fisher forecasting formalism to obtain a set of cross-correlated constraints on the two most widely-studied MG models in the literature, the

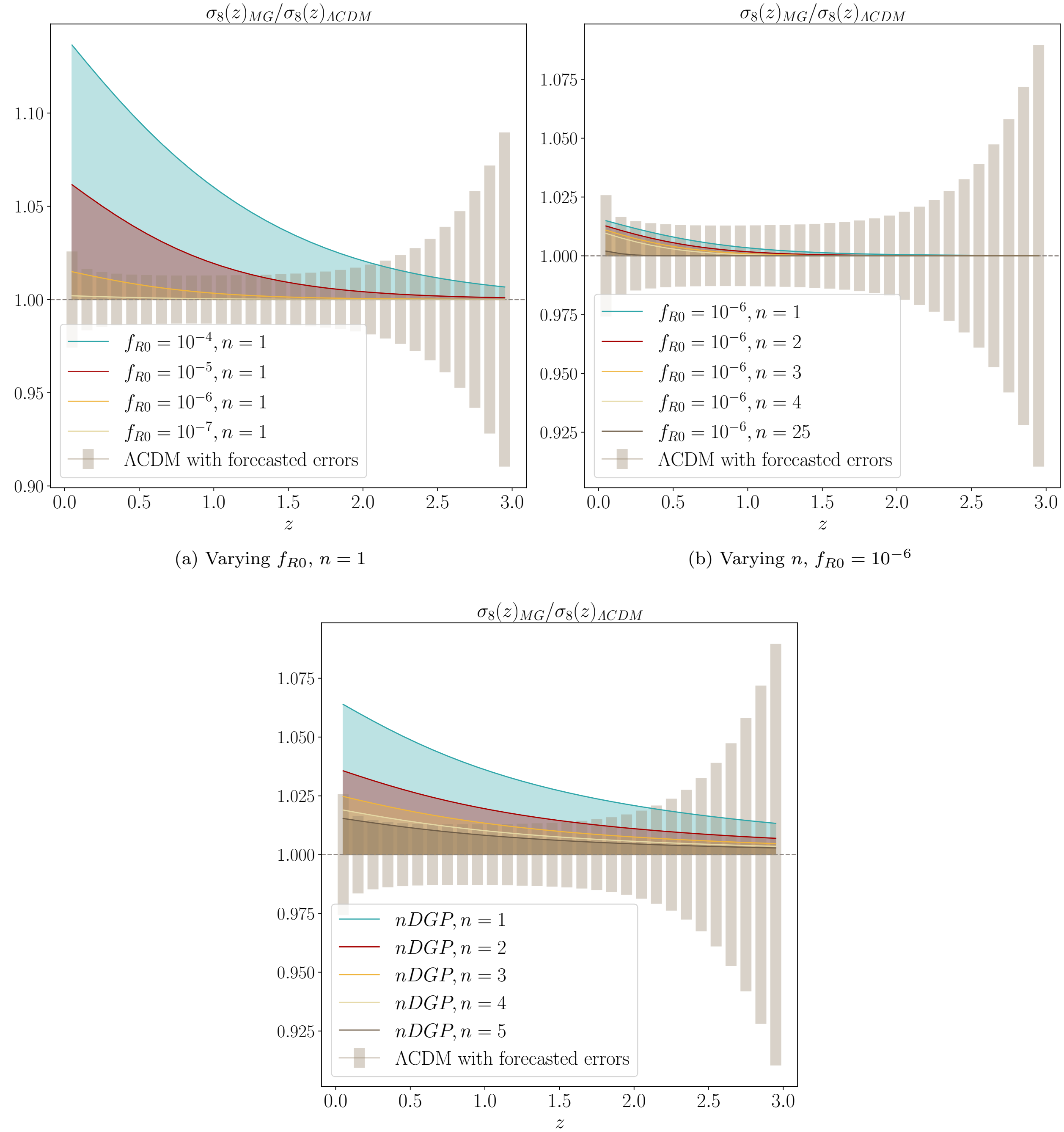

(a) Varying f_{R0}, $n = 1$

(b) Varying n, $f_{R0} = 10^{-6}$

(c) Varying n (nDGP)

FIG. 4. The MG predicted $\sigma_8(z)_{\rm MG}/\sigma_8(z)_{\Lambda\rm CDM}$ normalized at $z = 10$, plotted against the error of this ratio forecasted by cluster abundances. (a) shows the scenario with different f_{R0} values while fixing n in $f(R)$ as 1. (b) shows the opposite, fixing $f_{R0} = 10^{-6}$ while changing n. (c) shows the case in nDGP, where n_{DGP} is varied. This motivates our further Fisher analysis.

f(R) Hu-Sawicki and the nDGP gravity model. We demonstrate that the two independent probes complement each other harmonically in constraining the f(R) Hu-Sawicki model parameters, for varying degrees of deviation away from a ΛCDM background, as well as in a near-GR fiducial scenario. We find that the tightest constraints are obtained in the large-deviation F5 scenario, at the level of a $\sim 2\%$ forecasted joint constraint on the f_{R0} parameter, with the ELGs serving as the primary source of discriminating power on the galaxy clustering side. The constraining power of both probes is primarily derived from their corresponding lower redshift

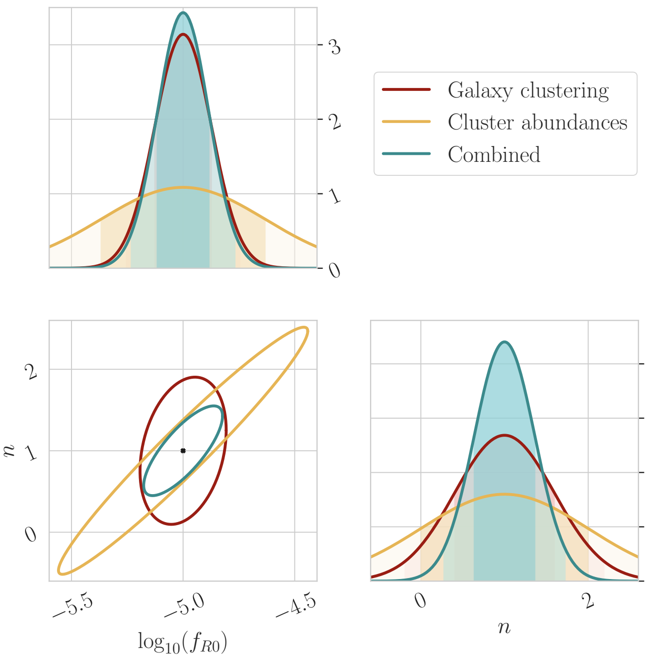

(a) F5 case (fiducial value 10^{-5})

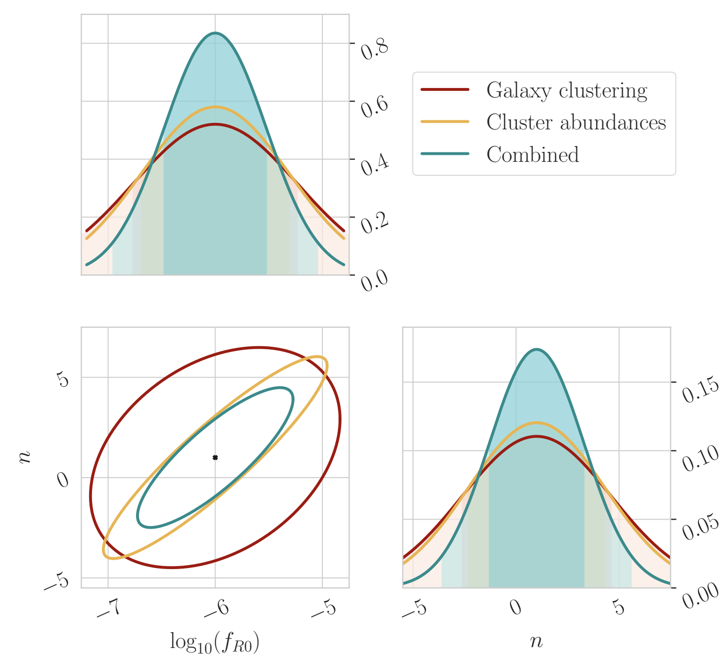

(b) F6 case (fiducial value 10^{-6})

FIG. 5. The combined Fisher constraints of $\log_{10}(f_{R0})$ and n using σ_8 for fiducial values $f_{R0} = 10^{-5}$ and 10^{-6}, with $n = 1$. Both the covariance ellipse regarding the two parameters and the respective one-parameter gaussian plots are included in each of the cases.

Model	Fiducial Parameters	Galaxy clustering			Cluster Abundances	Combined
		LRG	ELG	ELG+LRG		
$f(R)$	$\log_{10}(f_{R0}) = -5$	0.28	0.15	0.14	0.37	0.12
	$n = 1$	2.14	0.75	0.59	1.00	0.36
	$\log_{10}(f_{R0}) = -6$	1.78	1.12	0.77	0.69	0.48
	$n = 1$	8.64	5.92	3.61	3.31	2.30
	$f_{R0} = 0$	8.93×10^{-7}	5.77×10^{-7}	4.32×10^{-7}	3.77×10^{-7}	2.84×10^{-7}
DGP	$n_{DGP} = 1$	0.59	0.25	0.23	0.094	0.087
	$n_{DGP} = 5$	8.30	3.63	3.29	1.77	1.56

TABLE II. Marginalized one-parameter errors in MG models, presented using cluster abundances and galaxy clustering alone respectively, and cross-combining the two observables. The numerical values within the same row of a fiducial parameter denotes the $1-\sigma$ errors on the same parameter around that fiducial value.

snapshots, when the MG deviations are overall more pronounced. Our work is the first one in the literature, to the best of our knowledge, that presented constraints on the full 2D parameter space of the Hu-Sawicki model.

In a similar manner as in the f(R) case, we find that the interplay between the two observables can be utilized in order to also probe the parameter space of the nDGP gravity scenario, predicting a combined relative constraint of 2% in the $n = 1$ case. Having explored constraints to the two most widely-studied screening mechanisms in the literature, we highlight our ability to reliably explore the diverse landscape of MG theories.

Moving forward, there are many possible ways in which one can expand upon this line of work. On the galaxy clustering side, the accuracy of our model can be further improved by including the 1-loop corrections of Lagrangian PT [44] into the GSM prediction, as well as by introducing effective field theory corrections to account for non-perturbative small-scale physics. Such an approach would also need to be combined with a suitably improved treatment of the clustering covariance matrix, that we assumed to be Gaussian in the present work. Furthermore, it would be very interesting to also explore the constraining power of the Fourier space counterpart of the two-point function, the redshift space power spectrum, obtained either by analytical approaches (see e.g.

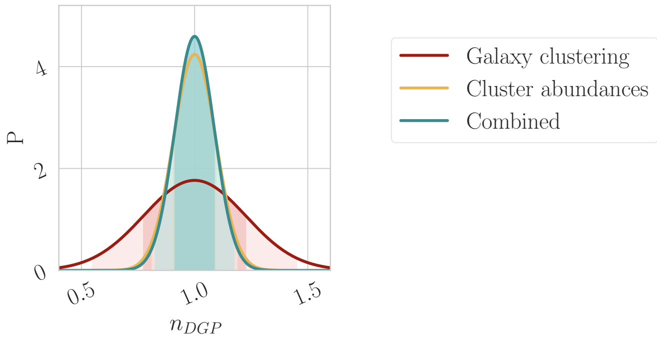

(a) $n = 1$ for nDGP

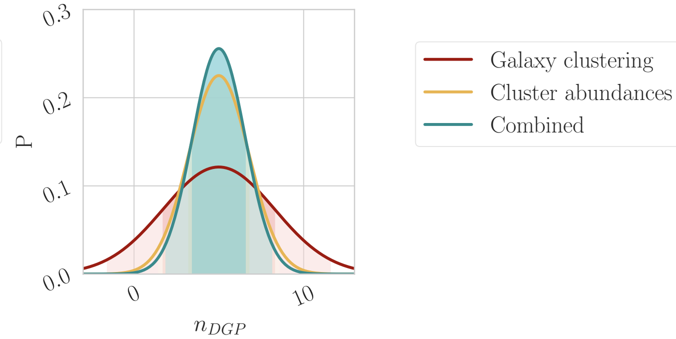

(b) $n = 5$ for nDGP

FIG. 6. The combined constraints for the Fisher forecast of n in the nDGP model for fiducial values $n = 1$ and $n = 5$.

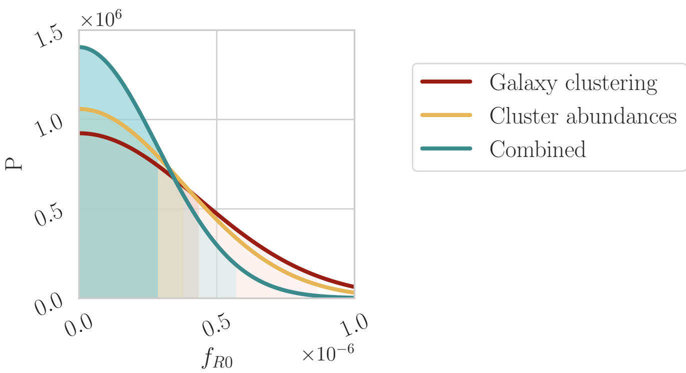

FIG. 7. The one-sided Gaussian error plot for the Fisher forecast with the fiducial value $f_{R0} = 0$. The value of n becomes redundant.

[55]) or through emulators [14]. Last but not least, it is tempting to explore how these constraints can further tighten through combinations with photometric and weak gravitational lensing observations by Stage-IV surveys such as the V. Rubin Observatory LSST [56, 57], using a Markov Chain Monte Carlo approach.

In the near future, powerful synergies between tremendous observational endeavors will allow the us to explore the vast landscape of dark energy and modified gravity parametrizations and obtain decisive answers on the nature of cosmic acceleration. Our work serves to highlight the great promise held in such considerations, as well as the optimal ways in which the vast amounts of upcoming observations could be utilized.

ACKNOWLEDGMENTS

The work of Rachel Bean and Georgios Valogiannis is supported by DoE grant DE-SC0011838, NASA ATP grant 80NSSC18K0695, NASA ROSES grant 12-EUCLID12-0004 and funding related to the Roman High Latitude Survey Science Investigation Team. Georgios Valogiannis' work is also supported by NSF grant AST-1813694.

APPENDIX

Appendix A: Covariance matrix calculation

In this Appendix, we provide the details of the analytical model we use to evaluate the covariance matrix of the multipoles of the anisotropic correlation function. We begin with the known expression for the Poisson error matrix of the power spectrum, assuming Gaussian density perturbations, which is the following [58, 59]:

$$
\begin{aligned}
&Cov\left[P(\mathbf{k}), P(\mathbf{k}')\right] = \\
&\frac{(2\pi)^3}{V_s}\left(P(\mathbf{k}+\frac{1}{n}\right)^2 \left(\delta_D(\mathbf{k}-\mathbf{k}') + \delta_D(\mathbf{k}+\mathbf{k}')\right) \\
&+ \frac{1}{n^2 V_s}\left[P(|\mathbf{k}-\mathbf{k}'|) + P(|\mathbf{k}+\mathbf{k}'| + 2P(\mathbf{k}) + 2P(\mathbf{k}')\right] \\
&+ \frac{1}{n^3 V_s},
\end{aligned} \tag{A1}
$$

with n the number density of the galaxies in a given sample, V_s the survey of the volume and δ_D the Dirac function. The second and third lines on the r.h.s of eq. (A1) encode the Poisson shot noise contributions to the covariance matrix [60]. Eq. (A1) has neglected contributions from nonlinear gravitational evolution [59, 61–63], super sample covariance [64–68] and effects of the survey nontrivial window function [69].

Our goal is to Fourier transform the result (A1), so that we obtain the configuration space equivalent expression for the covariance matrix of the anisotropic correlation function. In the simpler case of real space considerations, with the correlation function being isotropic, [60] demonstrated that, by angle-averaging the Fourier transform of (A1), the oscillatory Bessel function dependencies can be eliminated (unlike in the RSD case, as we will see below), and a more compact expression is possible. The same work also found the Poisson shot-noise contributions to be diagonal for the correlation function. In redshift space, which is what we are interested in, the equivalent configuration space expression for (A1) has been derived in [70, 71], assuming only Gaussian shot-noise contributions (i.e. neglecting the second and third lines in the r.h.s of (A1)), and is the following:

$$
\begin{aligned}
&Cov\left[\xi_{l_1}(s_i), \xi_{l_2}(s_j)\right] = \\
&\frac{i^{l_1+l_2}}{2\pi^2}\int_0^\infty k^2 \sigma^2_{l_1 l_2}(k) j_{l_1}(ks_i) j_{l_2}(ks_j) dk,
\end{aligned} \tag{A2}
$$

where we defined the multipole per-mode covariance:

$$
\begin{aligned}
\sigma^2_{l_1 l_2}(k) = &\frac{(2l_1+1)(2l_2+1)}{V_s} \\
&\times \int_{-1}^{1}\left[P(k,\mu_k) + \frac{1}{n}\right]^2 L_{l_1}(\mu_k) L_{l_2}(\mu_k) d\mu_k,
\end{aligned} \tag{A3}
$$

where $j_{l_1}(ks_i), j_{l_2}(ks_j)$ are the spherical Bessel functions of the first kind. Poisson shot-noise contributions can potentially become significant, as pointed out by [60]. To that end, we proceed to expand the expression (A2) to also include the Poisson terms to the shot-noise contributions, just like in the real-space version of [60]. To do so, we first start by adopting our convention for the Fourier transformation, applied on the correlation function:

$$
\xi(\mathbf{s}) = \int \frac{d^3k}{(2\pi)^3} e^{i\mathbf{k}\cdot\mathbf{s}} P(\mathbf{k}), \tag{A4}
$$

and label the terms reflecting the Poisson shot-noise contributions in (A1) (second and third lines of r.h.s) as $Cov\left[P(\mathbf{k}), P(\mathbf{k}')\right]\Big|_{\text{Poisson}}$. Fourier transforming both sides then gives [1]:

$$
\begin{aligned}
&Cov\left[\xi(\mathbf{s}_i), \xi(\mathbf{s}_j)\right]\Big|_{\text{Poisson}} = \\
&\frac{2}{n^2 V_s}\xi(\mathbf{s}_i)\delta_D(\mathbf{s}_i - \mathbf{s}_j).
\end{aligned} \tag{A5}
$$

Finally, we want to project out the correlation function multipoles, for which we integrate the ξ terms on the l.h.s above (after multiplying both sides with the appropriate Legendre polynomials), as in (23), which gives

$$
\begin{aligned}
&Cov\left[\xi_{l_1}(s_i), \xi_{l_{2j}}(s_j)\right]\Big|_{\text{Poisson}} = \\
&\frac{(2l_1+1)(2l_2+1)}{n^2 V_s 4\pi s_i^2}\delta_D(s_i - s_j)\int_{-1}^{1}\xi(s_i,\mu_s) L_{l_1}(\mu_s) L_{l_2}(\mu_s) d\mu_s,
\end{aligned} \tag{A6}
$$

where we have additionally made use of the delta function property:

$$
\delta_D(\mathbf{s}_i - \mathbf{s}_j) = \frac{\delta_D(s_i - s_j)}{s_i^2}\delta_D(\Omega_i - \Omega_j), \tag{A7}
$$

with Ω denoting the corresponding solid angles. Combining (A6) with (A2), we finally arrive at the desired result:

$$
\begin{aligned}
&Cov\left[\xi_{l_1}(s_i), \xi_{l_2}(s_j)\right] = \\
&\frac{i^{l_1+l_2}}{2\pi^2}\int_0^\infty k^2 \sigma^2_{l_1 l_2}(k) j_{l_1}(ks_i) j_{l_2}(ks_j) dk + \\
&\frac{(2l_1+1)(2l_2+1)}{n^2 V_s 4\pi s_i^2}\delta_D(s_i - s_j)\int_{-1}^{1}\xi(s_i,\mu_s) L_{l_1}(\mu_s) L_{l_2}(\mu_s) d\mu_s,
\end{aligned} \tag{A8}
$$

which is the equation we use to evaluate the covariance matrix of the multipoles of ξ in this work. The last term in eq. (A8) expands the Gaussian expression (A2) of [70, 71], in order to also capture the Poisson shot-noise contributions in the anisotropic case, and exhibits the

[1] The Fourier transformation of the r.h.s gives rise to additional terms involving δ functions, as in [60], that only contribute at separations $r = 0$, and are thus dropped.

same diagonal nature as the corresponding real space expression of [60] (eq. 32 in that work), which it recovers in the limit of isotropy. It is the first time, to the best of our knowledge, that this term is explicitly derived in the anisotropic case. The shot-noise terms in (A8) are further divided by the bin windth, Δs, in order to avoid overestimating the error predictions [2], as in [60, 73].

To summarize, after getting an analytical prediction for the RSD correlation function for our desired cosmology from eq. (17), we use it to predict the covariance matrix from eq. (A8) (combined with the input from (A3)). An intermediate step is to Fourier Transform to also get $P(k, \mu_k)$ from $\xi(s, \mu_s)$, which is required in eq. (A3), and can be easily performed with the publicly available package `mcfit` [3]. The integrals involving spherical Bessel functions in (A2) can be conveniently performed by utilizing the same package.

[1] W. Hu and I. Sawicki, Models of f(r) cosmic acceleration that evade solar-system tests 10.1103/PhysRevD.76.064004 (2007), arXiv:0705.1158.

[2] G. Dvali, G. Gabadadze, and M. Porrati, 4d gravity on a brane in 5d minkowski space 10.1016/S0370-2693(00)00669-9 (2000), arXiv:hep-th/0005016.

[3] M. Madhavacheril, N. Battaglia, and H. Miyatake, Fundamental Physics from Future Weak-Lensing Calibrated Sunyaev-Zel'dovich Galaxy Cluster Counts 10.1103/PhysRevD.96.103525 (2017), arXiv:1708.07502.

[4] M. Levi *et al.* (DESI collaboration), The DESI Experiment, a whitepaper for Snowmass 2013, (2013), arXiv:1308.0847 [astro-ph.CO].

[5] M. A. Mitchell, J. hua He, C. Arnold, and B. Li, A general framework to test gravity using galaxy clusters i: Modelling the dynamical mass of haloes in $f(r)$ gravity 10.1093/mnras/sty636 (2018), arXiv:1802.02165.

[6] D. S. Y. Mak, E. Pierpaoli, F. Schmidt, and N. Macellari, Constraints on modified gravity from sunyaev-zeldovich cluster surveys 10.1103/PhysRevD.85.123513 (2011), arXiv:1111.1004.

[7] P. Brax, C. van de Bruck, A.-C. Davis, and D. J. Shaw, f(R) Gravity and Chameleon Theories, Phys. Rev. **D78**, 104021 (2008), arXiv:0806.3415 [astro-ph].

[8] J. Khoury and A. Weltman, Chameleon cosmology, Phys. Rev. D **69**, 044026 (2004).

[9] J. Khoury and A. Weltman, Chameleon fields: Awaiting surprises for tests of gravity in space, Phys. Rev. Lett. **93**, 171104 (2004).

[10] C. Burrage and J. Sakstein, Tests of chameleon gravity, Living Reviews in Relativity **21**, 1 (2018), arXiv:1709.09071 [astro-ph.CO].

[11] H. Desmond and P. G. Ferreira, Galaxy morphology rules out astrophysically interesting $f(R)$, arXiv e-prints , arXiv:2009.08743 (2020), arXiv:2009.08743 [astro-ph.CO].

[12] T. Clifton, P. G. Ferreira, A. Padilla, and C. Skordis, Modified Gravity and Cosmology, Phys. Rept. **513**, 1 (2012), arXiv:1106.2476 [astro-ph.CO].

[13] M. Ishak *et al.*, Modified Gravity and Dark Energy models Beyond $w(z)$CDM Testable by LSST, (2019), arXiv:1905.09687 [astro-ph.CO].

[2] However, as pointed out by [71, 72], not averaging out the terms involving the spherical Bessel functions, in addition to the shot noise terms, will also lead to a degree of overestimation in the estimated covariances. In that regard, our predictions using this approach are more conservative.

[3] `https://github.com/eelregit/mcfit`

[14] N. Ramachandra, G. Valogiannis, M. Ishak, and K. Heitmann (LSST Dark Energy Science), Matter Power Spectrum Emulator for f(R) Modified Gravity Cosmologies, (2020), arXiv:2010.00596 [astro-ph.CO].

[15] A. Vainshtein, To the problem of nonvanishing gravitation mass, Physics Letters B **39**, 393 (1972).

[16] E. Babichev and C. Deffayet, An introduction to the Vainshtein mechanism, Class. Quant. Grav. **30**, 184001 (2013), arXiv:1304.7240 [gr-qc].

[17] K. Koyama, Ghosts in the self-accelerating universe 10.1088/0264-9381/24/24/R01 (2007), arXiv:0709.2399.

[18] G.-B. Zhao, B. Li, and K. Koyama, N-body simulations for f(r) gravity using a self-adaptive particle-mesh code 10.1103/PhysRevD.83.044007 (2010), arXiv:1011.1257.

[19] A. Lewis, A. Challinor, and A. Lasenby, Efficient computation of CMB anisotropies in closed FRW models, Astrophys. J. **538**, 473 (2000), arXiv:astro-ph/9911177 [astro-ph].

[20] A. Lewis and S. Bridle, Cosmological parameters from CMB and other data: A Monte Carlo approach, Phys. Rev. D **66**, 103511 (2002), arXiv:astro-ph/0205436 [astro-ph].

[21] C. Howlett, A. Lewis, A. Hall, and A. Challinor, CMB power spectrum parameter degeneracies in the era of precision cosmology, **1204**, 027 (2012), arXiv:1201.3654 [astro-ph.CO].

[22] H. Winther, S. Casas, M. Baldi, K. Koyama, B. Li, L. Lombriser, and G.-B. Zhao, Emulators for the non-linear matter power spectrum beyond cdm 10.1103/PhysRevD.100.123540 (2019), code for linear perturbation in MG from `https://github.com/HAWinther/Codes/tree/master/solve_linear_pert_mg`, arXiv:1903.08798.

[23] E. V. Linder, Cosmic growth history and expansion history 10.1103/PhysRevD.72.043529 (2005), arXiv:astro-ph/0507263.

[24] G. Valogiannis and R. Bean, Convolution lagrangian perturbation theory for biased tracers beyond general relativity 10.1103/PhysRevD.99.063526 (2019), arXiv:1901.03763.

[25] G. Valogiannis, R. Bean, and A. Aviles, An accurate perturbative approach to redshift space clustering of biased tracers in modified gravity 10.1088/1475-7516/2020/01/055 (2019), arXiv:1909.05261.

[26] Ya. B. Zeldovich, Gravitational instability: An Approximate theory for large density perturbations, Astron. Astrophys. **5**, 84 (1970).

[27] A. Aviles and J. L. Cervantes-Cota, Lagrangian perturbation theory for modified gravity, Phys. Rev. **D96**, 123526 (2017), arXiv:1705.10719 [astro-ph.CO].

[28] A. Aviles, M. A. Rodriguez-Meza, J. De-Santiago, and J. L. Cervantes-Cota, Nonlinear evolution of initially biased tracers in modified gravity, JCAP **1811** (11), 013, arXiv:1809.07713 [astro-ph.CO].

[29] A. Aviles, J. L. Cervantes-Cota, and D. F. Mota, Screenings in Modified Gravity: a perturbative approach, Astron. Astrophys. **622**, A62 (2019), arXiv:1810.02652 [astro-ph.CO].

[30] N. Kaiser, On the spatial correlations of Abell clusters, The Astrophysical Journal **284**, L9 (1984).

[31] G. Efstathiou, C. S. Frenk, S. D. M. White, and M. Davis, Gravitational clustering from scale-free initial conditions, **235**, 715 (1988).

[32] V. Desjacques, D. Jeong, and F. Schmidt, Large-Scale Galaxy Bias, Phys. Rept. **733**, 1 (2018), arXiv:1611.09787 [astro-ph.CO].

[33] T. Matsubara, Nonlinear perturbation theory with halo bias and redshift-space distortions via the Lagrangian picture, Phys. Rev. **D78**, 083519 (2008), [Erratum: Phys. Rev.D78,109901(2008)], arXiv:0807.1733 [astro-ph].

[34] J. Carlson, B. Reid, and M. White, Convolution Lagrangian perturbation theory for biased tracers, Monthly Notices of the Royal Astronomical Society **429**, 1674 (2013), arXiv:1209.0780.

[35] Z. Vlah, M. White, and A. Aviles, A Lagrangian effective field theory, JCAP **1509** (09), 014, arXiv:1506.05264 [astro-ph.CO].

[36] Z. Vlah, E. Castorina, and M. White, The Gaussian streaming model and convolution Lagrangian effective field theory, JCAP **1612** (12), 007, arXiv:1609.02908 [astro-ph.CO].

[37] N. Kaiser, Clustering in real space and in redshift space, Monthly Notices of the Royal Astronomical Society **227**, 1 (1987), http://oup.prod.sis.lan/mnras/article-pdf/227/1/1/18522208/mnras227-0001.pdf.

[38] A. J. S. Hamilton, Measuring Omega and the real correlation function from the redshift correlation function, .

[39] A. J. S. Hamilton, Linear redshift distortions: A Review, in *Ringberg Workshop on Large Scale Structure Ringberg, Germany, September 23-28, 1996* (1997) arXiv:astro-ph/9708102 [astro-ph].

[40] K. B. Fisher, On the Validity of the Streaming Model for the Redshift-Space Correlation Function in the Linear Regime, The Astrophysical Journal, eprint = astro-ph/9412081, keywords = COSMOLOGY: LARGE-SCALE STRUCTURE OF UNIVERSE, COSMOLOGY: THEORY, GALAXIES: DISTANCES AND REDSHIFTS, year = 1995, month = aug, volume = 448, pages = 494, doi = 10.1086/175980, adsurl = https://ui.adsabs.harvard.edu/abs/1995ApJ...448..494F, adsnote = Provided by the SAO/NASA Astrophysics Data System.

[41] B. A. Reid and M. White, Towards an accurate model of the redshift-space clustering of haloes in the quasi-linear regime, Monthly Notices of the Royal Astronomical Society **417**, 1913 (2011).

[42] L. Wang, B. Reid, and M. White, An analytic model for redshift-space distortions, Mon. Not. Roy. Astron. Soc. **437**, 588 (2014), arXiv:1306.1804 [astro-ph.CO].

[43] R. Scoccimarro, Redshift-space distortions, pairwise velocities, and nonlinearities, Phys. Rev. D **70**, 083007 (2004).

[44] G. Valogiannis, R. Bean, and A. Aviles, An accurate perturbative approach to redshift space clustering of biased tracers in modified gravity, JCAP **01**, 055, arXiv:1909.05261 [astro-ph.CO].

[45] A. Font-Ribera, P. McDonald, N. Mostek, B. A. Reid, H.-J. Seo, and A. Slosar, DESI and other dark energy experiments in the era of neutrino mass measurements, JCAP **05**, 023, arXiv:1308.4164 [astro-ph.CO].

[46] N. Mostek, A. L. Coil, M. Cooper, M. Davis, J. A. Newman, and B. J. Weiner, The DEEP2 Galaxy Redshift Survey: Clustering Dependence on Galaxy Stellar Mass and Star Formation Rate at z ~1, Astrophys. J. **767**, 89 (2013), arXiv:1210.6694 [astro-ph.CO].

[47] T. Lazeyras, C. Wagner, T. Baldauf, and F. Schmidt, Precision measurement of the local bias of dark matter halos, JCAP **02**, 018, arXiv:1511.01096 [astro-ph.CO].

[48] H. Mo and S. D. White, An Analytic model for the spatial clustering of dark matter halos, Mon. Not. Roy. Astron. Soc. **282**, 347 (1996), arXiv:astro-ph/9512127.

[49] H. Mo, Y. Jing, and S. White, High-order correlations of peaks and halos: A Step toward understanding galaxy biasing, Mon. Not. Roy. Astron. Soc. **284**, 189 (1997), arXiv:astro-ph/9603039.

[50] M. Davis and P. J. E. Peebles, A survey of galaxy redshifts. V - The two-point position and velocity correlations, The Astrophysical Journal **267**, 465 (1983).

[51] J. A. Peacock, Errors on the measurement of ? via cosmological dipoles, Monthly Notices of the Royal Astronomical Society **258**, 581 (1992), http://oup.prod.sis.lan/mnras/article-pdf/258/3/581/3777991/mnras258-0581.pdf.

[52] A. Albrecht, L. Amendola, G. Bernstein, D. Clowe, D. Eisenstein, L. Guzzo, C. Hirata, D. Huterer, R. Kirshner, E. Kolb, and R. Nichol, Findings of the joint dark energy mission figure of merit science working group (2009), arXiv:0901.0721.

[53] D. Coe, Fisher matrices and confidence ellipses: A quick-start guide and software (2009), arXiv:0906.4123.

[54] B. Bose, M. Cataneo, T. Tröster, Q. Xia, C. Heymans, and L. Lombriser, On the road to per-cent accuracy IV: ReACT – computing the non-linear power spectrum beyond ΛCDM, (2020), arXiv:2005.12184 [astro-ph.CO].

[55] A. Aviles, G. Valogiannis, M. A. Rodriguez-Meza, J. L. Cervantes-Cota, B. Li, and R. Bean, Redshift space power spectrum beyond Einstein-de Sitter kernels, (2020), arXiv:2012.05077 [astro-ph.CO].

[56] P. A. Abell *et al.* (LSST Science Collaborations, LSST Project), LSST Science Book, Version 2.0, (2009), arXiv:0912.0201 [astro-ph.IM].

[57] A. Abate *et al.* (LSST Dark Energy Science), Large Synoptic Survey Telescope: Dark Energy Science Collaboration, (2012), arXiv:1211.0310 [astro-ph.CO].

[58] H. A. Feldman, N. Kaiser, and J. A. Peacock, Power spectrum analysis of three-dimensional redshift surveys, Astrophys. J. **426**, 23 (1994), arXiv:astro-ph/9304022.

[59] A. Meiksin and M. J. White, The Growth of correlations in the matter power spectrum, Mon. Not. Roy. Astron. Soc. **308**, 1179 (1999), arXiv:astro-ph/9812129.

[60] J. D. Cohn, Power spectrum and correlation function errors: Poisson vs. Gaussian shot noise, New Astron. **11**, 226 (2006), arXiv:astro-ph/0503285.

[61] R. Scoccimarro, M. Zaldarriaga, and L. Hui, Power spectrum correlations induced by nonlinear clustering, Astrophys. J. **527**, 1 (1999), arXiv:astro-ph/9901099.

[62] A. Cooray and W. Hu, Power spectrum covariance of

weak gravitational lensing, Astrophys. J. **554**, 56 (2001), arXiv:astro-ph/0012087.
[63] A. Barreira and F. Schmidt, Response Approach to the Matter Power Spectrum Covariance, JCAP **11**, 051, arXiv:1705.01092 [astro-ph.CO].
[64] A. J. Hamilton, C. D. Rimes, and R. Scoccimarro, On measuring the covariance matrix of the nonlinear power spectrum from simulations, Mon. Not. Roy. Astron. Soc. **371**, 1188 (2006), arXiv:astro-ph/0511416.
[65] W. Hu and A. V. Kravtsov, Sample variance considerations for cluster surveys, Astrophys. J. **584**, 702 (2003), arXiv:astro-ph/0203169.
[66] M. Takada and W. Hu, Power Spectrum Super-Sample Covariance, Phys. Rev. D **87**, 123504 (2013), arXiv:1302.6994 [astro-ph.CO].
[67] Y. Li, M. Schmittfull, and U. Seljak, Galaxy power-spectrum responses and redshift-space super-sample effect, JCAP **02**, 022, arXiv:1711.00018 [astro-ph.CO].
[68] A. Barreira, E. Krause, and F. Schmidt, Complete super-sample lensing covariance in the response approach, JCAP **06**, 015, arXiv:1711.07467 [astro-ph.CO].
[69] Y. Li, S. Singh, B. Yu, Y. Feng, and U. Seljak, Disconnected Covariance of 2-point Functions in Large-Scale Structure, JCAP **01**, 016, arXiv:1811.05714 [astro-ph.CO].
[70] M. White, B. Reid, C.-H. Chuang, J. L. Tinker, C. K. McBride, F. Prada, and L. Samushia, Tests of redshift-space distortions models in configuration space for the analysis of the BOSS final data release, Mon. Not. Roy. Astron. Soc. **447**, 234 (2015), arXiv:1408.5435 [astro-ph.CO].
[71] J. N. Grieb, A. G. Sánchez, S. Salazar-Albornoz, and C. Dalla Vecchia, Gaussian covariance matrices for anisotropic galaxy clustering measurements, Mon. Not. Roy. Astron. Soc. **457**, 1577 (2016), arXiv:1509.04293 [astro-ph.CO].
[72] A. G. Sánchez, C. M. Baugh, and R. Angulo, What is the best way to measure baryonic acoustic oscillations?, Monthly Notices of the Royal Astronomical Society **390**, 1470 (2008), https://academic.oup.com/mnras/article-pdf/390/4/1470/3022373/mnras0390-1470.pdf.
[73] R. E. Smith, R. Scoccimarro, and R. K. Sheth, Motion of the acoustic peak in the correlation function, Phys. Rev. D **77**, 043525 (2008).